Fabrication and characterization of CVD grown 2D materials

Maaz Ahmed Qureshi

Master Thesis Report

April 2020

Department of Physics and Mathematics
University of Eastern Finland

Maaz Ahmed Qureshi *Fabrication and characterization of CVD grown 2D materials*, 48 pages
University of Eastern Finland
Master's Degree Programme in Photonics

Supervisor Prof. Harri Lipsanen
Prof. Markku Kuittinen

Abstract

Two dimensional (2D) materials have attracted extensive attention in the field of semiconductor industry due to their excellent properties of high conductivity, high mobility, and suitable bandgap, combined with thin and flexible structure. Although graphene has exhibited exceptional properties in various applications, researchers focused also on other 2D materials such as dichalcogenides for the operation of field-effect transistors (FETs) due to their suitable energy bandgaps. Because better quality and high efficiency transistors are typically demanded in electronics applications, this thesis examines the synthesis and characterization of various 2D materials suitable for FET device applications.

In this work, thin layers of MoS_2, CrS_2, FeS_2, and TiS_2 were synthesized using chemical vapor deposition process at various suitable parameters of temperatures, pressures and gas flow rates, and these materials were further characterized using SEM-EDS, Micro-Raman and Linkam measurement setups. SEM and Raman analysis showed that a thin layer can be synthesized at the annealing temperature of 750 °C using the CVD process. Furthermore, electron beam lithography was used to fabricate the FET devices for each synthesized 2D material.

Optical characterizations were also performed to determine the effectiveness of fabricated FET devices for various applications. Photoluminescence (PL) measurements at various cryogenic temperatures were also performed and discussed in the report. PL measurements showed that the spectrum broadens and peak wavelength shifts to longer wavelengths as the temperature is increased from -196 °C to +23 °C. As an outlook, research and development still continues to discover and synthesize other 2D materials which have even better optical response for various applications.

Keywords: Two dimensional (2D) materials; chemical vapor deposition; transition metal dichalcogenides; Molybdenum disulphide.

Contents

Chapter I

Introduction

The field-effect transistors (FETs), the backbone of the semiconductors electronics, are considered as the building blocks of communication and information technology. Thus, increasing the efficiency and performance of the FET transistors is at the focus to continue the progress in these critical fields of research and development. For this purpose, two dimensional materials have attracted much attention from the transistor community after the successful preparation of graphene samples in 2004 [1, 2]. Although graphene was expected to be a perfect channel material for FETs because of its high carrier mobility, it could not live up to the high expectations since it does not possess a bandgap that is required for the proper operation of FETs [3]. After realizing that graphene cannot be a key channel material in transistors, the quest continued for the exploration of other two dimensional (2D) materials which could have inherent energy bandgap suitable for the transistor operations. Thus, transition metal dichalcogenides (TMDs), gallium nitride, black phosphorus, etc. were extensively explored and, in 2011, the first field-effect transistors based on MoS_2 material were reported [4–7].

Fabrication of a monolayer MoS_2 based FET provided new momentum for 2D materials and, within a short period of time, different novel 2D materials such as MoS_2, $MoSe_2$, WS_2, WSe_2 and others were also discovered and synthesized [8]. A monolayer of these 2D materials provided the bandgap that is essential for transistor operation. These materials were promising not only because of their high electron mobility and bandgap but also because of their very thin structure that make them favorable for the applications in thin and flexible electronics [9].

The theoretical electron mobility of single-layered MoS_2 transistors is about 320

$cm^2V^{-1}s^{-1}$. Compared to the current on/off ratio of copper sulfide which is approximately 1 x 10^4, a thin layer of MoS_2 has a current on/off ratio of up to 1 x 10^8 at room temperature and pressure, which is an advantage for the electrostatic control over the conduction channel in the 2D materials [7, 8, 10]. Because of their thin structure, they can be electrically biased easily and can also operate at low voltages. Thus, these materials also provide promising applications in the field of superconductors, solar cells, LEDs, etc.

Because of the success of the FET transistors based on MoS_2, research based on other 2D materials also accelerated. Although other 2D materials such as CrS_2, FeS_2, and TiS_2 were also explored and appreciated, the quest for the synthesis of better efficiency and quality of these 2D materials still continues [11]. For this purpose, we synthesized various 2D materials (MoS_2, CrS_2, FeS_2, and TiS_2) using chemical vapor deposition (CVD) process and performed characterization of these materials using scanning electron microscopy and micro-Raman tools. Optical characterization was also performed in order to determine their effectiveness for optoelectronic applications.

The basic theory of 2D materials, along with the discussion of the fabrication and characterization tools, is presented in chapter 2. Since the synthesis of materials is the first experimental step toward applications, the process of growth and synthesis of the mentioned 2D materials, along with our experimental fabrication of FET transistors using these 2D materials, is detailed comprehensively in chapter 3. Chapter 4 discusses the characterization and experimental results of these 2D materials. Starting from the initial characterization of SEM-EDS and Raman analysis, the optical characterization of these various 2D materials have also been discussed. Some of the characterizations have never been performed before, so they certainly demanded extensive research and analysis. Variation of the parameters in the CVD process was performed in order to try to increase the quality of the synthesized single-layer two dimensional materials. Finally, the significant outputs of this work have been discussed and concluded at the end of this report.

Chapter II

Theory

In the previous chapter, we discussed the significance of 2D materials for FETs. The first part of this chapter is focused on the basic theory and concept of two dimensional materials. To determine the quality and effectiveness of the synthesized 2D materials using several characterization tools, the later part of this chapter presents various characterization tools necessary to characterize the synthesized 2D materials and explore their optical properties.

2.1 Two-dimensional (2D) materials

Referred to as thin-layered materials, 2D materials are crystalline materials which consists of a few or a single layer of atoms. 2D materials can usually be categorized as either compounds (with two or more covalently bounded elements, such as MoS_2) or as 2D allotropes of a single element (such as carbon in its allotrope graphene) [12]. Although almost 700 different 2D materials have been predicted to be stable, graphene and transition metal dichalcogenides (TMDs) are some of the most well-known 2D materials presently available and synthesized [13, 14]. These materials have remarkable applications in the field of semiconductors, detectors, emitters, photovoltaics, battery energy, electrodes etc. and the global market is expected to reach over USD 390 million by 2025 [15, 16].

While graphene was the first 2D material that was isolated in 2004, there have been several other 2D materials researched and synthesized, showing a wide range of properties [12, 13]. This report focuses on the synthesis of TMDs using CVD, their optical characterization and their applications in fabrication of devices such as FET transistors. Unlike graphene that has zero bandgap and thus low current on/off ratio

in transistor applications, some TMDs monolayers are also structurally stable and display suitable bandgaps [17]. Because of their high electron mobility comparable to that of silicon, they can be effectively used for the fabrication of transistors [17].

TMDs have chemical formula MX_2, where M is the transition metal (such as molybdenum (Mo), iron (Fe), chromium (Cr), titanium (Ti), etc.) and X is a chalcogen (such as sulfur (S), selenium (Se), etc.). Depending on the different TMDs, the crystal structure can be varied. While most common crystal structure is of trigonal symmetry, which is possessed for example by MoS_2, WS_2, $MoSe_2$, some TMDs can also possess hexagonal crystal structure [11]. These semiconductors have van der Waals bonds between layers and have an indirect energy bandgap when synthesized in bulk [18]. Each layer consists of a metal layer that is sandwiched between two chalcogenide layers [18]. However, for monolayers, their bandgap becomes direct and typically in the visible spectrum [19]. Because of their attractive charge mobility and optical properties, monolayer 2D materials are a popular choice for fabrication of detectors and transistors in optoelectronics.

2.2 Fabrication and characterization tools and material's growth processes

The synthesis of 2D materials is the first step to fabricate any transistor devices based on 2D materials. In order to synthesize suitable monolayers of transition metal dichalcogenides, we have used chemical vapor deposition process and experiment with multiple parameters in the process. After successful growths, the thin films of 2D materials are transferred onto Si/SiO_2 substrate and various characterizations are performed. Since the FET device fabrication uses electron beam lithography (EBL), EBL setup and optical characterization tools have also been discussed. Thus, chemical vapor deposition process, scanning electron microscopy, micro-Raman, EBL and Linkam measurement setup are described in this chapter.

2.2.1 Chemical vapor deposition process

Chemical vapor deposition (CVD) growth of TMDs can be traced back to 1988 when MOCVD growth of MoS_2 and WS_2 on various substrates were demonstrated [20]. The primary aim of the CVD growth of TMDs is to prepare single crystal TMD atomic layers and grow single or few-layered sheets. Although there exist other methods for synthesis of 2D materials, such as mechanical exfoliation, and liquid phase routes, CVD growth technique offers higher efficiency than mechanical exfoliation and better quality control than liquid phase routes [20]. Therefore, CVD is typically considered as a reliable growth technique for the preparation of high quality 2D materials.

CVD is a process to deposit films of materials in a gaseous phase by the chemical reaction of the volatile precursors and the surface of the substrate. As vapor of precursors passes over the surface of the heated substrate, a chemical reaction takes place and a solid phase of desired chemicals are deposited onto the substrate. Due to the high temperature reactions, some volatile by-products are also produced which are usually removed by the gas flow through the other end of the CVD chamber.

CVD synthesis of 2D materials typically involves chemical reactions of precursors in a specially-designed environment known as CVD furnace. To obtain the desired chemicals on the substrate, various furnace parameters need to be considered: furnace temperature, pressure, gas flow rate, etc. For example, temperature of the CVD furnace is highly critical to determine the proper chemical reaction of

precursors with the surface of the substrate. The image of the CVD furnace and setup used for our experiment is represented in Figure 2.1.

The CVD process is widely used in semiconductor industry to deposit materials in various forms, including: epitaxial, amorphous, monocrystalline, polycrystalline, etc. [11]. These materials can include graphene, sulphides, nitrides, selenides, tellurides, oxynitrides, etc. [11].

Figure 2.1: CVD Furnace including the chamber, heater, pressure and air flow controller.

2.2.2 Scanning electron microscopy and energy-dispersive X-ray spectroscopy

Scanning electron microscope (SEM), shown in Figure 2.2a, is a specific type of electron microscope that scans the surface of a material using a focused beam of electrons to produce a high quality image. The electrons in the focused beam interact with the atoms in the materials and produces various signals depending on the material's composition. These output signals from the sample also contain vital information regarding the surface topography of the constituent materials in the sample. The focused beam of electrons scans the sample in a raster scan pattern and the intensity of the detected signal obtained at various positions of the beam produces an accurate image at a nanoscale level.

Energy-dispersive X-ray spectroscopy (EDS) is a technique used for the chemical characterization of the sample. Each element in a sample has a unique atomic structure that causes unique set of peaks on the emitted electromagnetic spectrum when the beam of electrons interacts with the sample, inducing X-ray emission that is detected by a detector. Thus, this tool works primarily on the principle of spectroscopy.

In EDS, as the beam of electrons is focused onto the sample, an unexcited electron at the ground state in the discrete energy levels is excited and ejected from the shell while creating an electron vacancy in the location of that electron in the ground state. A higher-energy electron from the outer shell then fills that vacancy, and the energy difference between the lower-energy shell and the higher-energy shells is released in the form of an X-ray. And an energy-dispersive spectrometer then measures the energy and number of X-rays emitted from the sample [21]. Thus, the elemental composition of the sample is measured as the energies of the X-ray are characteristic of the atomic structure and the energy difference between the two higher and lower shells of the emitting element [21]. This working principle is represented in Figure 2.2b. Therefore, the main components of the EDS setup are: excitation source (electron beam), X-ray detector, pulse processor, and analyzer.

(a) (b)

Figure 2.2: (a) Image of a scanning electron microscope (SEM) including (EDS). (b) Representation of the emission of X-rays by the beam of incoming electron in (EDS).

2.2.3 Micro-Raman

Micro-Raman tool (shown in Figure 2.3) works on the main principle of Raman spectroscopy which originates from the inelastic scattering of light by matter. Electromagnetic energy, such as laser light, reflects, absorbs, transmits, and scatters when it interacts with a material. One specific type of scattering is Raman scattering and it enables the identification of vibrational modes of molecules in the sample. The Raman spectrum allows to identify the elemental composition of materials in the sample. Thus, Raman scattering acts as the basis for Raman spectroscopy and the micro-Raman tool.

Monochromatic light using a laser source is used to excite the electrons, and scattered light is detected by very sensitive detectors. The laser light is focused on the material through a microscope lens and sub-micrometer regions in the sample can be analyzed. The scattered light from the sample is usually analyzed in terms of the frequency shift with respect to the laser wavelength, with additional information obtained from the frequency-shift dependent intensity of the detected light. The

peaks in the spectrum of this scattered detected light corresponds to vibration modes of the various materials or elements present in the sample analyzed.

Raman spectroscopy has applications in a very wide range of fields including nanotechnology, optoelectronics, semiconductors, polymers, transmission, biology, geology, etc. [22]. In nano-technology, micro-Raman is used to analyze elemental compositions in a material, and the same setup allows to study also the photoluminescence (PL) response of that material to the incident laser light. In the experimental work discussed in this report, the micro-Raman tool has been used to analyze the PL response as well as Raman response to obtain the material composition of various 2D materials.

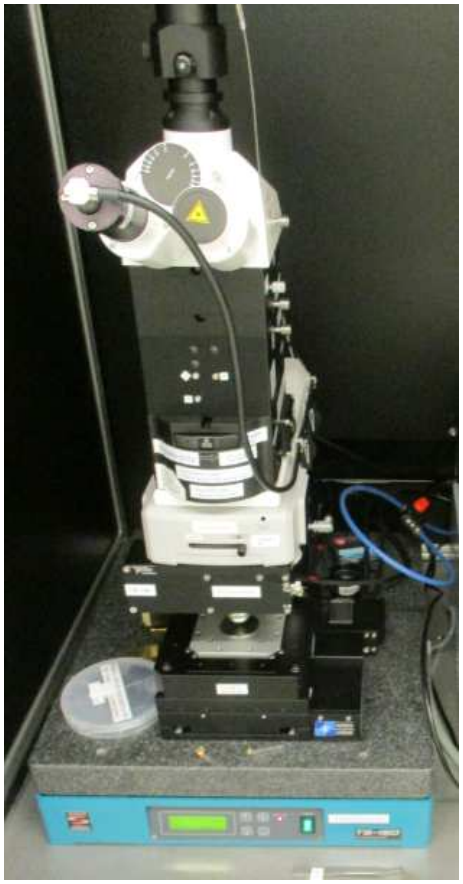

Figure 2.3: Image of a Micro-Raman used for Raman spectroscopy and optical characterization.

2.2.4 Electron beam lithography

Electron beam lithography (EBL) stems out of scanning electron microscopy where a beam of electrons is focused on the samples to create custom shape nanostructures on the surfaces covered with an electron-sensitive film called resist [23]. EBL was initially suggested in 1958, and the proper demonstration was done in 1960 [24]. Powerful EBL systems can achieve high quality resolutions down to a few nanometers. Patterns are designed using suitable computer-aided design (CAD) tools and then the beam of focused electrons is moved over the sample to record that previously prepared design on the resist that was deposited onto the sample using the spin coating and baking process [24].

The solubility of the resist is changed by the electron beam, and it enables the selective removal of exposed or non-exposed regions of the resist as it is immersed in a suitable solvent. In the successive development steps, either the unexposed material is removed (negative-tone process) or the exposed material is removed (positive-tone process) to make a patterned film that acts as a suitable binary mask for further processing. This binary mask enables various processes to be performed such as physical vapor deposition, reactive ion etching, electroplating, etc. [24]. Thus, several valuable electronic devices can be fabricated efficiently.

Electron beam lithography provides a vast range of nano-patterning application in the fields of photonics, telecom industry, nano-fabrication, quantum technologies, etc. [25]. This technique can produce devices such as transistor gates, laser gratings, imprint masks, photonic crystals, optical elements, and many more. In the experimental work discussed in this report, EBL technique is used to pattern and fabricate the transistor gates (gate, source and drain contacts in FET transistors) onto our 2D material samples. By using these gates, electrical characterization can be performed to determine the efficiency of the transistors produced using various 2D materials. The setup of electron beam lithography is represented in Figure 2.4.

Figure 2.4: Image of a 100 keV beam energy EBL Vistec for lithography.

2.2.5 Linkam measurement setup

Linkam equipment is used to characterize the samples in the field of microelectronics and semiconductors. Many device applications require the spectroscopic and microscopic observations to extract the values and the variation of electrical and optical parameters of devices. Linkam electrical and optical measurement setup provides a controlled environment for these measurements. Accurate temperature between -196 °C to 600 °C through cooling with liquid nitrogen or heating, along with vacuum, humidity levels, and gas flow, is also easily controllable.

Linkam probe stage was used with electrical and gas connections and needle probes to measure the optical properties at cryogenic temperatures (down to -196 °C). Thus, various optical characteristics of the 2D materials can be determined as a function of temperature. Moreover, Linkam setup is also compatible with spectroscopy and microscopy techniques including, but not limited to, Raman spectroscopy, PL measurements, etc. The experimental work mentioned in this report has performed optical characterization of various 2D materials using this Linkam measurement setup shown in Figure 2.5.

Figure 2.5: Image of a Linkam equipment THMS600 - heating and cooling stage.

Chapter III

Fabrication of 2D materials

In chapter 2, we discussed the general fabrication and characterization tools usually used to synthesize and characterize the 2D materials for FET device applications. In this chapter we focus on the detailed experimental process and precise parameters and specifications that we have used to synthesize, pattern and characterize our various fabricated FETs. This chapter starts with the discussion of the fabrication of different metal-gold alloys by the evaporator process before continuing with the synthesis of various 2D materials using CVD process. Further, the synthesized CVD based 2D materials were transferred onto Si/SiO_2 substrates before the FET connectors were patterned using electron beam lithography to perform various characterizations.

3.1 Fabrication of M-Au Alloy by the Evaporator

CVD growth process for two dimensional compounds using metal catalysts that was published earlier require that both M (a transition metals such as Mo, Cr, Fe, or Ti) and X (a chalcogen such as S) be insoluble in the catalyst to ensure surface-limited growth [26–28]. A single component solid solution was prepared by alloying gold (Au) of different thickness on the metal (M) film that has limited solubility of the X element. A thin layer of the transition metal M (approx. 20 nm thick) was sputtered onto a c-plane sapphire substrate which was followed by thick layers of gold deposition on its surface by heating the M-Au layer to 850 °C to form an alloy with the Au by the Evaporator tool. The tool used to prepare the M-Au alloy is known as Evaporator e-gun Edwards which prepared the alloy using the physical vapor deposition technique.

The concentration of M in the final alloy is determined by the relative thickness of the M and Au layers and the concentration of M is intentionally kept limited to less than 5 % in order to maintain single-phase alloying conditions. Using the evaporator, alloys of different relative thickness of M-Au (e.g. 1 %, 2 %, 3 % and 4 %) were prepared to later grow the monolayers using the CVD process. In our experimental work, we have prepared four different alloys (such as Mo-Au, Cr-Au, Fe-Au, Ti-Au) with different relative thickness of M-Au using the evaporator tool. These alloys of different relative thicknesses were used in the CVD process with 'S' as (chalcogen) to synthesize different 2D materials.

3.2 Synthesis of MoS_2, CrS_2, FeS_2, TiS_2 by CVD process

Chemical vapor deposition (CVD) was used to synthesize different transition metal dichalcogenides (TMDs) by using metal-organic precursor which are chalcogenated at elevated temperatures in the furnace to form 2D materials on the substrate. This transition to synthesize thin film 2D material by CVD process from M-Au (e.g. Mo) on sapphire substrate produced by the evaporation process in represented in Figure 3.1.

The furnace is heated to high temperatures of around $600 - 900$ °C with an inert gas argon flowing through the tube at a fixed flow rate. For proper reaction, some materials also require H_2 gas as a catalyst to be flowing through the furnace tube in small quantities [29]. This chemical vapor deposition process is usually preferred over the mechanical exfoliation technique because it can produce larger and more uniform surface areas, that is, larger continuous flakes [20, 30].

Because of the limited solubility of X in the Au, a few atomic layers of the compound are expitaxially aligned to the underlying gold sapphire substrate as M-Au alloy is exposed to the simple vapor-phase precursor of X. For the experimental work, we have used MTI corp. OTF-1200X CVD furnace with 60 mm diameter quartz tube in which vacuum level can reach up to 10^{-2} torr while temperature can reach up to 1200 °C. For the synthsis of different 2D materials (MoS_2, CrS_2, FeS_2, TiS_2) in our experiment, maximum temperature, argon incoming flow, and vacuum pressure were set and controlled according to the specific compound (M-Au).

There are two heaters – right and left heaters – available in the CVD furnace: the right heater was used for the heating of M-Au, while the left heater was used for the

heating of X (such as sulphur). The sulphur in the left heater was usually introduced to the heated region of the left heater in the last 30 minutes of the annealing time. The temperature in the left heater was usually higher than 180 °C to vaporize the sulphur and argon gas flow assisted sulphur vapors to flow from the left heater to the right heater during the annealing time. The schematic of this CVD process is represented in Figure 3.2.

The samples were allowed to cooled down gradually afterwards and later taken out for various characterizations after the transfer process onto Si/SiO_2 substrate. Since the maximum temperature, annealing time, pressure, and gas flow rate are significant factors for high-quality synthesis of 2D materials, several attempts were required with various combinations of these factors in the CVD process for the optimization of 2D material systhesis.

Figure 3.1: Representation of thin film of MoS_2 2D material formation in the CVD process.

3.3 Transfer of MoS_2, CrS_2, FeS_2, TiS_2 materials onto the substrate

After synthesizing various 2D materials such as MoS_2 on Au sapphire substrate using CVD process, the thin layers of MoS_2 or other compounds need to be transferred onto Si/SiO_2 substrate. In order to do so, a PMMA resist layer is spin coated onto the sample, and later the sample of thin film on Au sapphire substrate is immersed in the potassium iodide (KI) acid for almost 48 hours. It will gradually dissolve the Au from the sample and thus only the thin layer of 2D material (e.g. MoS_2) would remain in the acid. That thin layer of material is then transferred from KI acid to the already patterned Si/SiO_2 P-doped substrate. This process of transferring

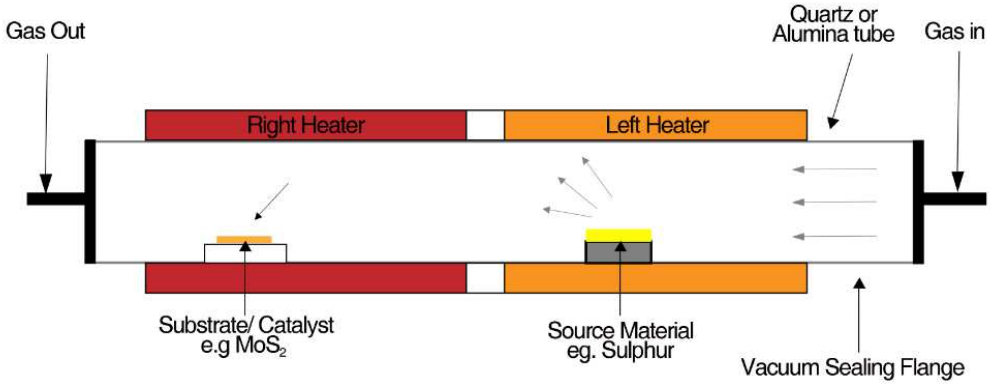

Figure 3.2: (a) Schematic diagram of our experimental CVD process for the synthesis of MoS_2, CrS_2, FeS_2, TiS_2 materials.

the 2D thin layer from the Au sapphire substrate to the Si/SiO_2 P-doped substrate, represented in Figure 3.3, was also used for the transfer of other 2D materials (e.g. MoS_2, CrS_2, FeS_2, TiS_2) as well.

The substrate was earlier patterned with Ti/Au markers using EBL. The approximately 500 μm thick crystalline Si substrate has approximately 285 nm thick SiO_2 layer on top. Before the process of transferring of 2D films on the Si/SiO_2 substrate, we patterned Ti/Au (5 nm /50 nm) markers on the 4 inch Si/SiO_2 substrate by EBL patterning and E-beam evaporation. These type of markers on the substrate make it easier to locate the transferred materials on the substrate, and according to that we can pattern the FET gate contacts on Si/SiO_2 substrate using EBL.

Figure 3.3: Transfer of two dimensional materials from M-Au sapphire substrate to the Si/SiO_2 substrate.

After transferring the 2D film onto the Si/SiO_2 substrate, this transferred sample

is immersed in water to remove the droplets of KI acid from the transferred sample. Using a nitrogen gun, the water droplets are removed from the sample as well. The sample is then submerged in the acetone for 10 minutes to dissolve the PMMA from the sample. Afterwards the sample is immersed in isopropanol (IPA) for almost 2 minutes to remove the acetone from the sample and again the nitrogen spray gun is used to remove the droplets of IPA from the sample as well. The sample of 2D material on the Si/SiO_2 substrate is now ready to be characterized using SEM-EDS, Raman, optical microscope, etc. However, patterning of FETs using EBL is required to perform the electrical characterization using Linkam measurement setup.

3.4 Patterning and fabrication of FET transistors using electron beam lithography

After transferring the thin films on the Si/SiO_2 substrate, we require to pattern the connectors of FET transistors (such as source, gate, drain) on the samples. These connectors can enable us to analyze the I-V characteristics and Hall effect of the FET transistors. The connectors were initially designed using CAD software and later patterned using EBL Vistec setup.

For resist coating on our sample of size 1.2 cm x 1.2 cm, we initially coated methyl methacrylate - MMA 8.5 - through spin coating process at 4000 rpm and then coated polymethyl methacrylate - PMMA A4.5 - through spin coating process at 2000 rpm. The approximate thickness of MMA layer is 300 nm, while the thickness of PMMA layer is 200 nm. After the resist coating, we patterned the sample with EBL using a current of 70 nA and a dose of 1200 $\mu C/cm^2$. Different connectors to the FET transistor were patterned on the sample, as represented in Figure 3.4. Using the same procedure, the sample of other 2D materials (MoS_2, CrS_2, FeS_2, and TiS_2) were also fabricated and patterned using EBL setup similarly.

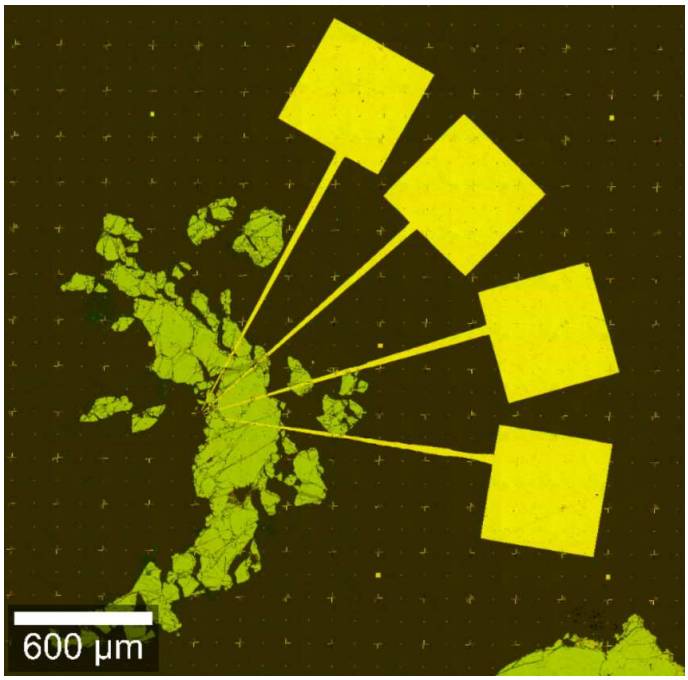

Figure 3.4: Representation of connectors of field-effect transistor patterned using EBL on an MX_2 material.

Chapter IV

Experimental results and characterization of 2D material

In the previous chapters, theory and experimental fabrication processes of 2D materials based transistors were discussed. The primary aim of this report is to determine and analyze the possibility and effectiveness of proper synthesis of 2D materials using CVD process. To determine the effectiveness of their synthesis, characterizations such as Raman, SEM and optical measurements were performed on various synthesized samples of MoS_2, CrS_2, FeS_2, TiS_2, and HfS_2 to analyze their feasibility in the application of FET transistors. Moreover, the experimental results are also discussed and compared with the earlier published and predicted results of the synthesis and photoluminescence measurements.

4.1 Raman and SEM analysis

Raman spectroscopy and SEM analysis are powerful tools for materials identifications in samples. In our experimental work, different samples of MoS_2, CrS_2, FeS_2, TiS_2, and HfS_2 were synthesized using different combinations of annealing temperatures, pressures, gas flow rates, etc. Several such combinations were experimented to optimize the synthesis process and later the samples were characterized to analyze the quality of their material growth. The following sections present the Raman and SEM analysis for various combinations of synthesis parameters for different materials.

4.1.1 MoS_2 samples

Although several combinations of parameters were experimented for the optimized synthesis of 2D MoS_2 materials, this section focuses on the Raman and SEM analysis of only three such combinations:

- **MoS_2 bulk material synthesized at the annealing temperature of 900 °C**

  This MoS_2 sample was synthesized at the annealing temperature of 900 °C with argon gas flow rate of 50 sccm using the CVD process. After the CVD synthesis, the film was transferred onto the Si/SiO_2 substrate and FET connectors were patterned using EBL Vistec tool. Raman and SEM analysis were performed afterwards and the stitching images captured by the Raman tool at two different points are represented in Figure 4.1.

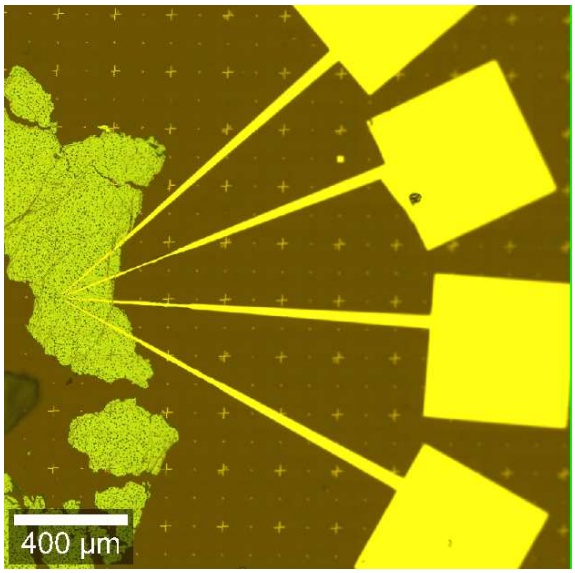

Figure 4.1: Stitching images of two different regions of MoS_2 bulk material synthesized at the annealing temperature of 900 °C.

Typical micro-Raman response from the MoS_2 material film is shown in Figure 4.2a. Earlier published papers have suggested that the predicted Raman peaks for bulk MoS_2 should be at 383 rel. cm^{-1} and 408 rel. cm^{-1} [31]. In our

experimentally synthesized MoS_2 material, Raman response at 380 rel. cm^{-1} and 406 rel. cm^{-1} is observed which is in good agreement with the anticipated results. The vertical axis represents the relative intensity while the horizontal axis of the Raman graphs represents the wave number. Our primary interest for the Raman analysis is on the positions of peaks on the horizontal axis since intensity is relative, and the relative intensity can be conveniently controlled by adjusting the laser power. Since the material film was transferred onto the Si/SiO_2 substrate, Figure 4.2b represents the Raman response taken on a substrate region with no film of MoS_2. Thus, the peaks on the Raman response are used to identify the materials grown.

A SEM image of a MoS_2 film captured using SEM EBL Zeiss Supra 40 is represented in Figure 4.3. For monolayers, we expect triangular-shaped for the flakes [11]. Here, the shapes of the flakes are not triangular because the grown material is bulk material. By adjusting and controlling the parameters in the CVD synthesis, the growth of MoS_2 was optimized and monolayers were also synthesized, as mentioned in the analysis of the other samples.

(a)

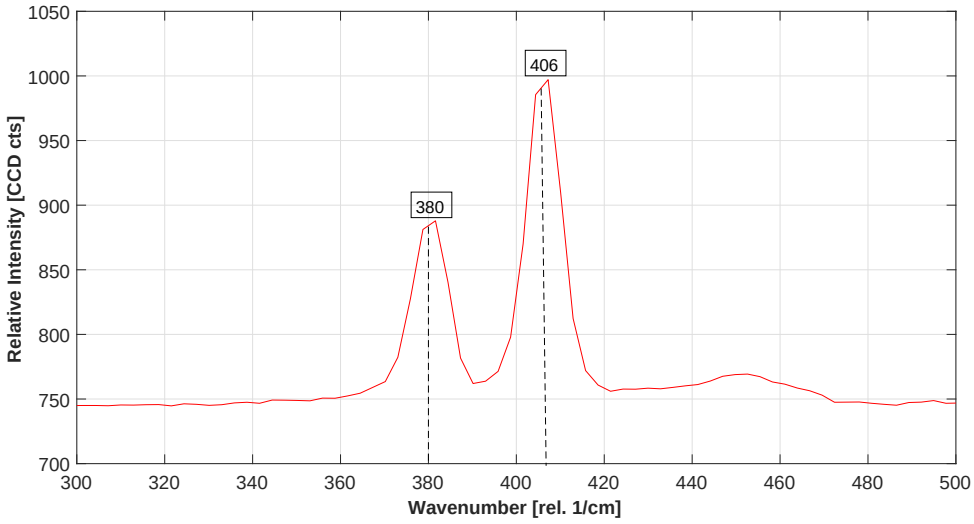

(b)

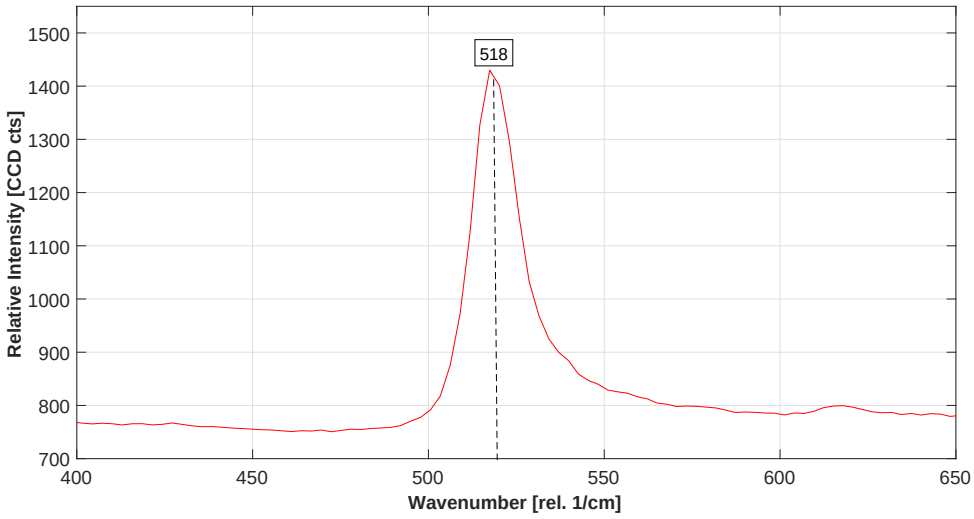

Figure 4.2: (a) Raman spectrum of MoS_2 material synthesized at the annealing temperature of 900 °C. (b) Raman spectrum of Si/SiO_2 substrate.

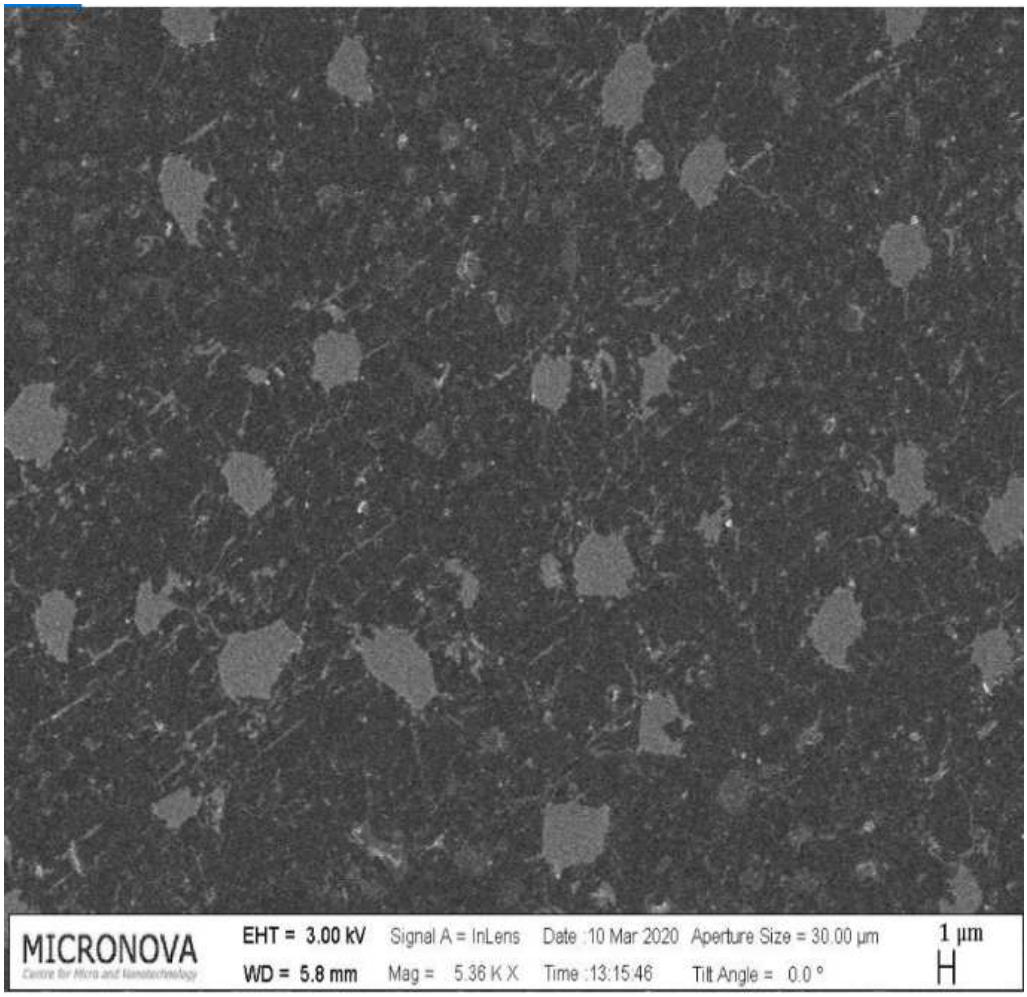

Figure 4.3: SEM image of bulk MoS_2 material synthesized at the annealing temperature of 900 °C.

- **MoS_2 thin film material synthesized at the annealing temperature of 750 °C**

  This MoS_2 monolayer was synthesized at the annealing temperature of 750 °C with an argon gas flow rate of 50 sccm using CVD process. Similar to the previously discussed sample, this sample was also transferred onto Si/SiO_2 substrate and patterned using EBL as represented by the stitching images shown in Figure 4.4. FET connectors on three different regions on the sample were patterned using EBL. It is beneficial to perform characterization at different areas on the sample to analyze the effect of material defects on the optical responses. For example, Figure 4.4a represents the regions with less material defects compared to Figure 4.4b.

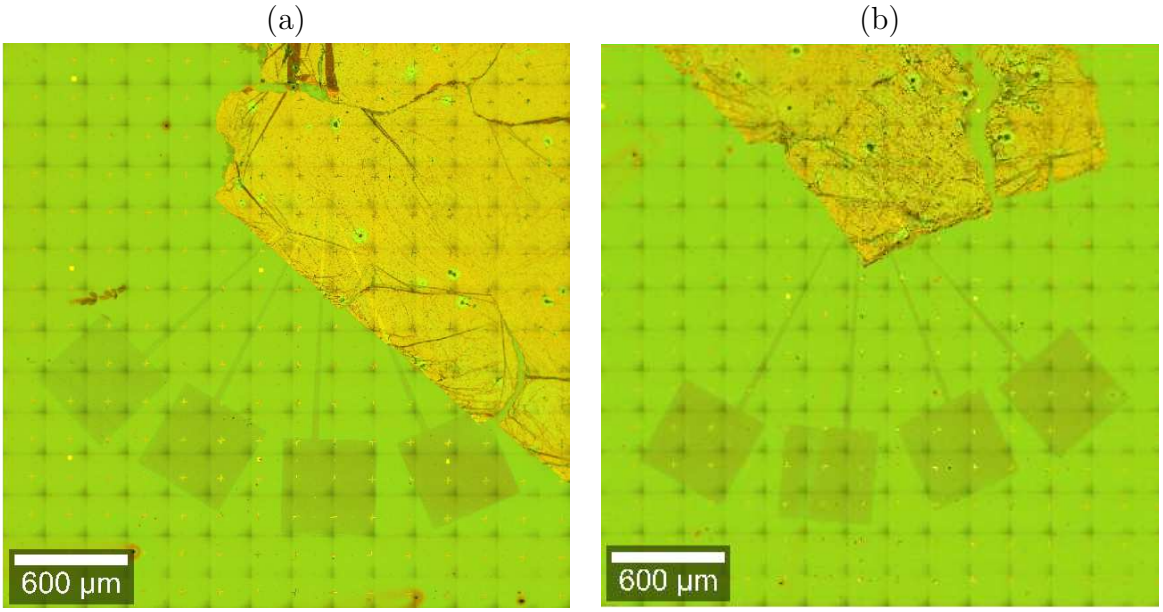

Figure 4.4: Stitching images of MoS_2 material synthesized at the annealing temperature of 750 °C with regions of a) low material defects b) high material defects.

Figure 4.5a represents the Raman response of this synthesized sample, and it can be observed that the Raman peaks are at 379 rel. cm^{-1} and 405 rel. cm^{-1}. According to the published paper, the Raman peaks for monolayers should be at 385 rel. cm^{-1} and 405 rel. cm^{-1} [31]. Thus, this result is in faily good

accordance with the expected results for the Raman analysis. Figure 4.5b represents the Raman response on Si/SiO_2 substrate without any material film.

The SEM image of thin-layered MoS_2 is represented in Figure 4.6. The triangular flakes represented in the figure confirm the growth of thin layers by the CVD process at the mentioned parameters of temperature, pressure, gas flow rate, etc. This result is also following the earlier published result where the experimental outcome showed that triangular-shaped flakes are obtained for the growth of few-layer MoS_2 materials. [11].

(a)

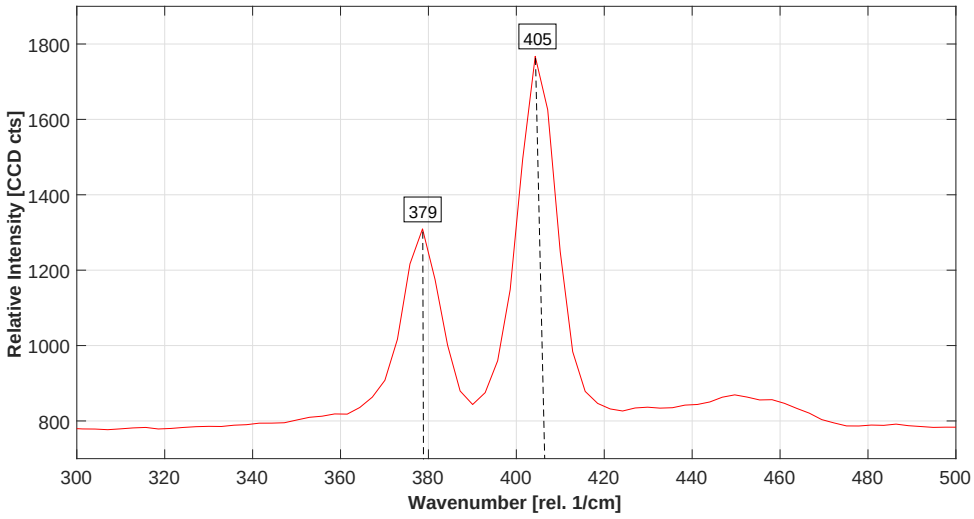

(b)

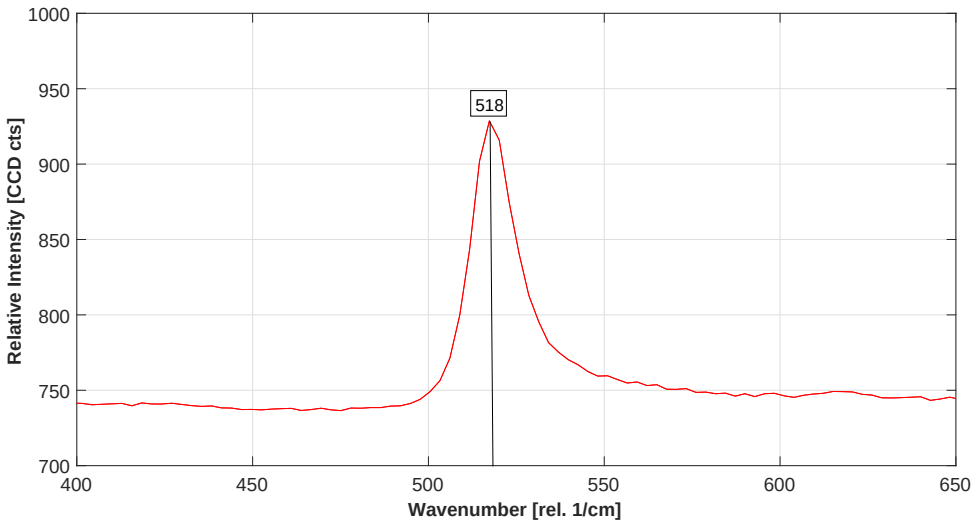

Figure 4.5: (a) Raman spectrum of MoS_2 material synthesized at the annealing temperature of 750 °C. (b) Raman spectrum of Si/SiO_2 substrate.

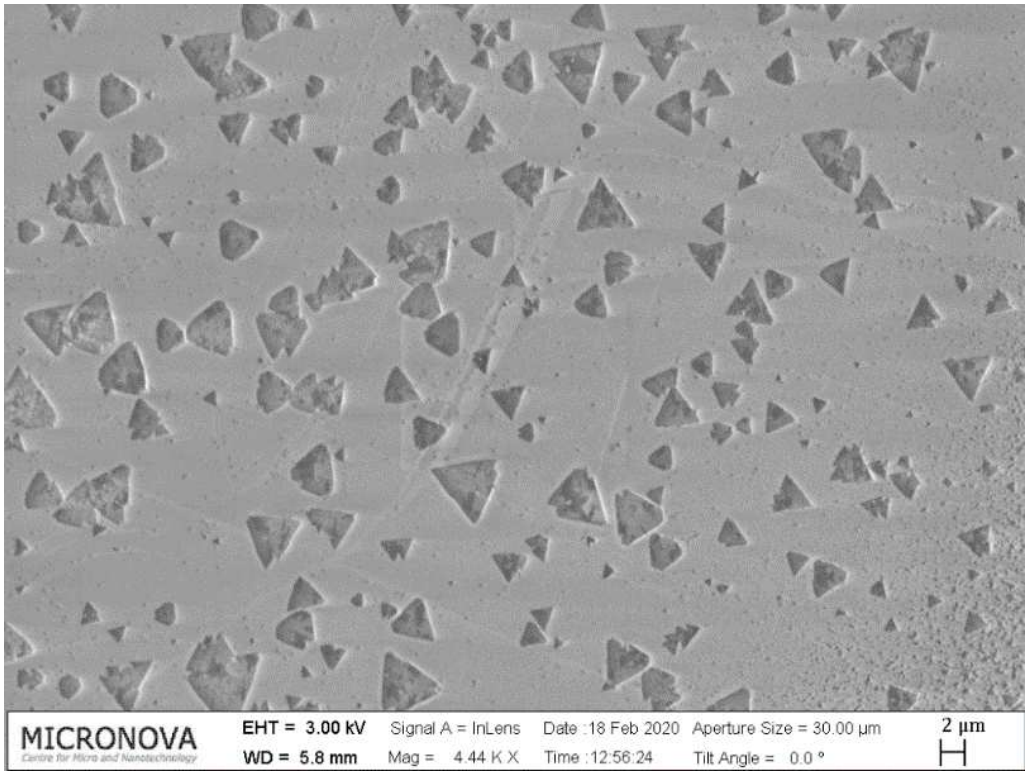

Figure 4.6: SEM image of a few-layer MoS_2 material synthesized at the annealing temperature of 750 °C.

- **MoS_2 thin film material synthesized at the annealing temperature of 800 °C**

  This thin layer of MoS_2 material was synthesized at the annealing temperature of 800 °C with an argon gas flow rate of 50 sccm. Again, connectors of FETs were patterned on the film and the stitching images are shown in Figure 4.7. As discussed earlier, performing characterizations at the connector points on this sample is also beneficial to analyze the quality of the synthesized material. Raman response on the film is represented in Figure 4.8a, while the Raman response of the underlying substrate of Si/SiO_2 is represented in Figure 4.8b. Thus, the Raman peak at 518 rel. cm^{-1} in Figure 4.8a is due to the underlying substrate. Moreover, since other Raman peaks are observed at 376 rel. cm^{-1} and 402 rel. cm^{-1}, it suggests that MoS_2 material was also synthesized properly by the CVD process.

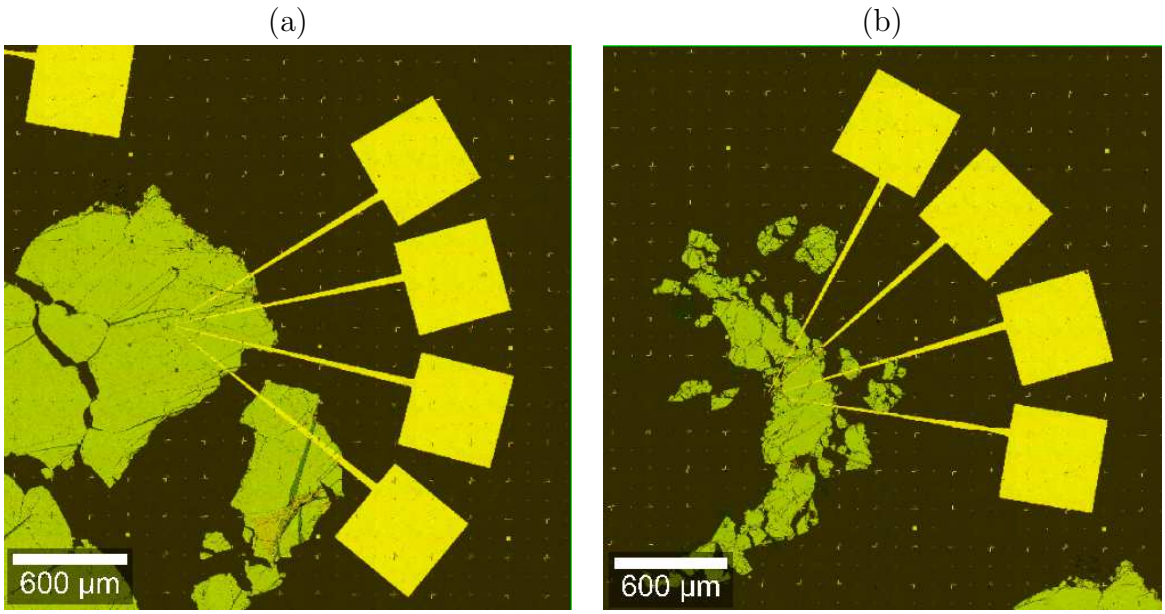

Figure 4.7: Stitching images of MoS_2 material synthesized at the annealing temperature of 800 °C with regions of (a) low material defects (b) high material defects.

(a)

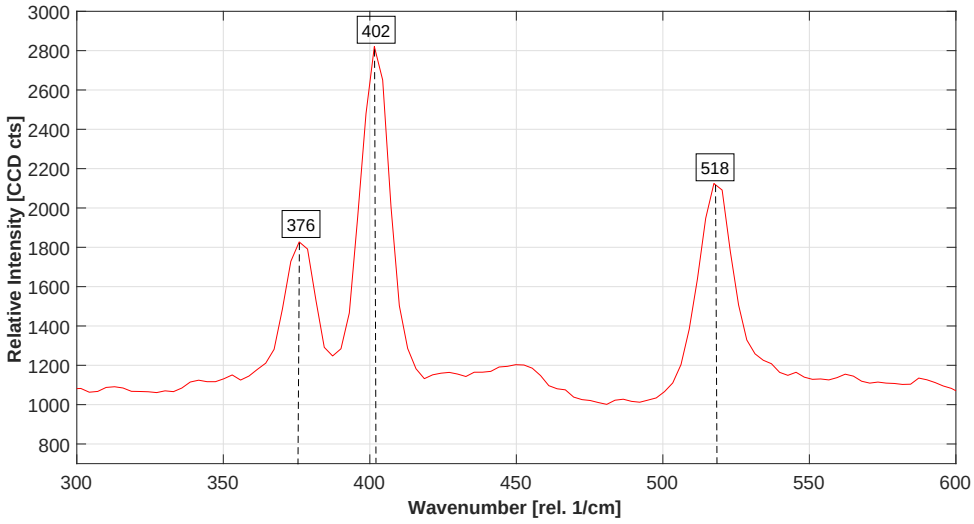

(b)

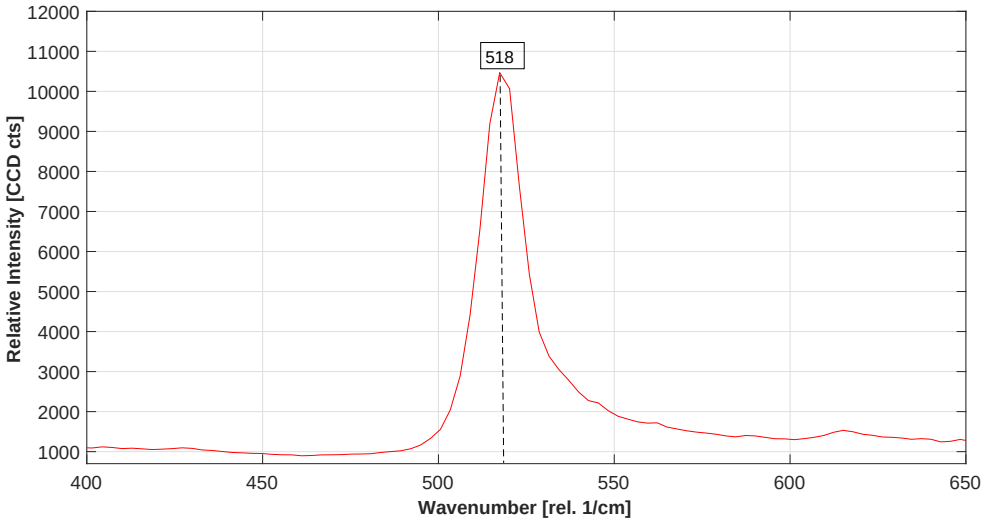

Figure 4.8: (a) Raman spectrum of MoS_2 material synthesized at the annealing temperature of 800 °C. (b) Raman spectrum of Si/SiO_2 substrate.

4.1.2 CrS_2 sample

Similar to the synthesis of MoS_2 samples, several parameters were tested during the CVD process to optimize the synthesis of CrS_2. However, this section has summarized and discussed the Raman and SEM analysis of only one such combinations.

CrS_2 thin film material synthesized at the annealing temperature of 800 °C
This CrS_2 sample was synthesized at the annealing temperature of 800 °C with the argon gas flow rate of 50 sccm during the CVD process. The stitching images of the synthesized CrS_2 film on the sapphire substrate captured by the Raman tool are represented in Figure 4.9. Raman response observed on the film is shown in Figure 4.10a, while Raman image scan captured by the Raman tool is represented in Figure 4.10b. The expected Raman peaks for CrS_2 material are at 254 rel. cm^{-1} and 286 rel. cm^{-1}. In our experimental results, the peaks at 256 rel. cm^{-1} are observed, This response suggests the growth of CrS_2 on sapphire substrate by the CVD process.

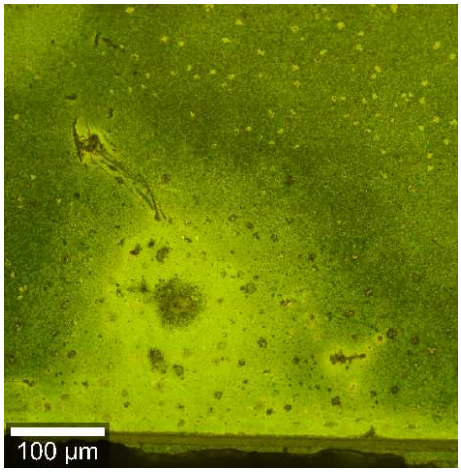

Figure 4.9: Stitching image of region of CrS_2 material synthesized at the annealing temperature of 800 °C.

The SEM image of CrS_2 is represented in Figure 4.11. According to the research published earlier, properly synthesized CrS_2 is expected to produce the triangular-flakes [11]. SEM characterization results have also observed few triangular-shaped flakes which are in accordance with the expected results.

(a)

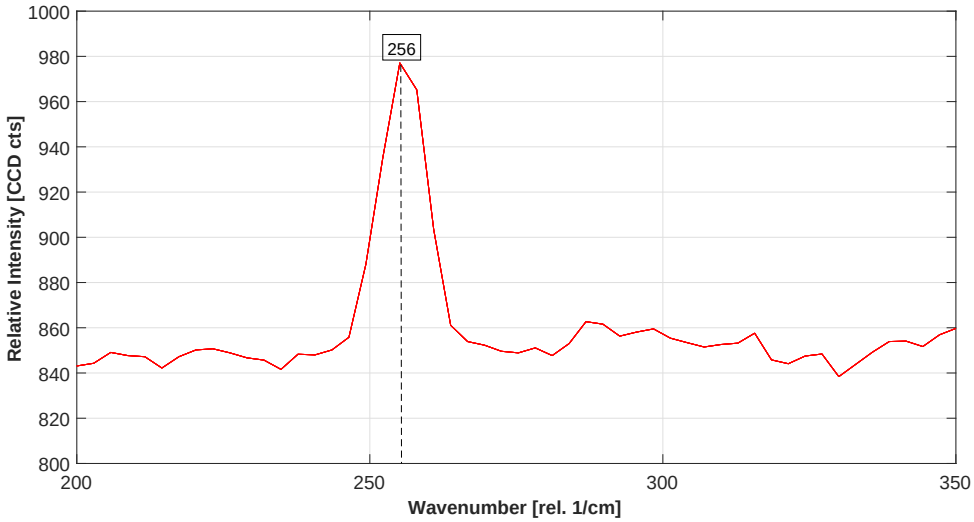

(b)

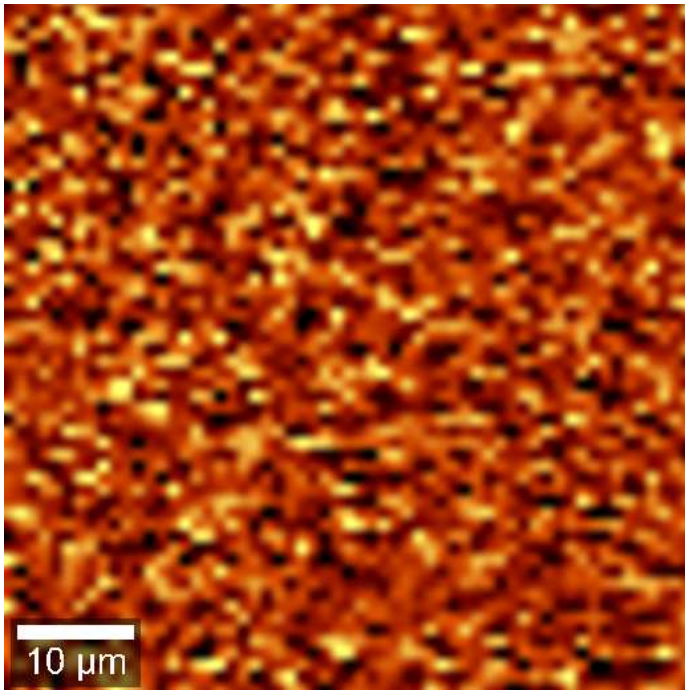

Figure 4.10: (a) Raman spectrum of CrS_2 material synthesized at the annealing temperature of 800 °C. (b) Raman image scan of CrS_2 sample captured by micro-Raman tool.

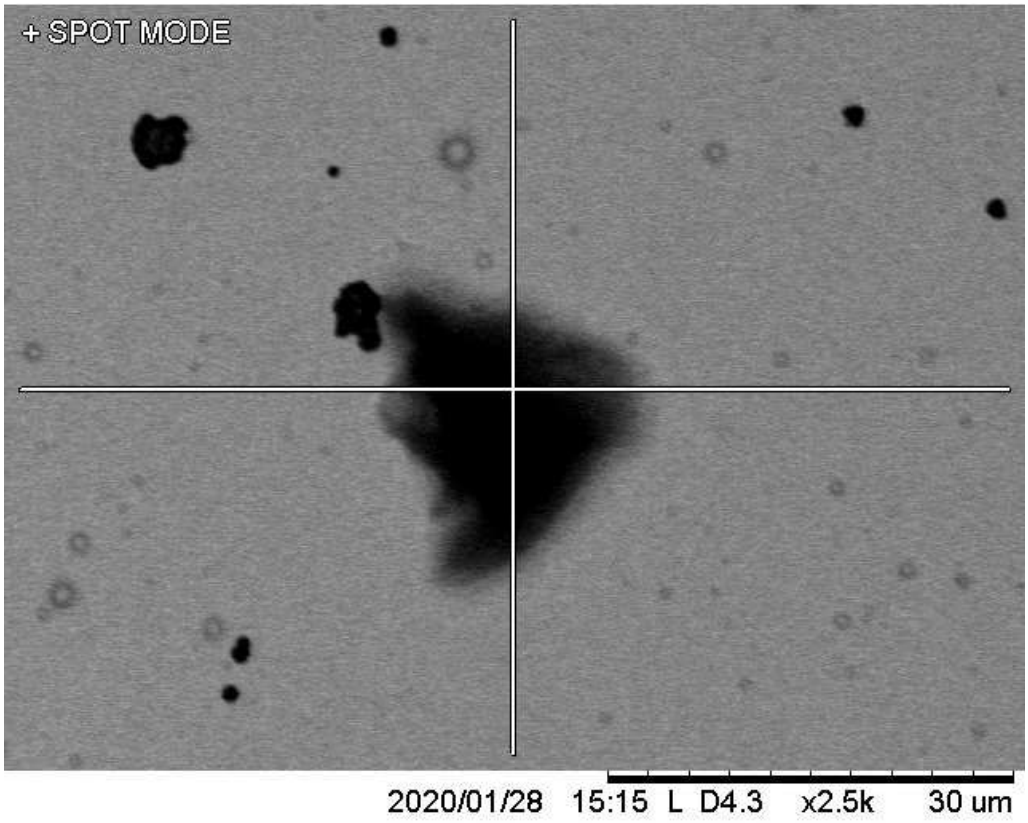

Figure 4.11: SEM image of CrS_2 material synthesized at the annealing temperature of 800 °C.

4.1.3 FeS_2 samples

While several parameters were tested during the CVD process for the synthesis of FeS_2 as well, this section focuses on the Raman and SEM analysis of only one such combination.

FeS_2 thin film material synthesized at the annealing temperature of 800 °C
This FeS_2 sample was synthesized at the annealing temperature of 800 °C with argon gas flow rate of 50 sccm during the CVD process. The stitching images of the synthesized FeS_2 film on the sapphire substrate captured by the Raman tool are represented in Figure 4.12. These two different images represent the two regions of different thickness of gold on iron. The Raman response observed at any arbitrary point on the sample is represented in Figure 4.13. The expected Raman peaks for FeS_2 material are at 337 rel. cm^{-1} and 372 rel. cm^{-1} [32]. Experimental results have observed the peaks at 342 rel. cm^{-1} and 377 rel. cm^{-1}, and this confirms the growth of FeS_2 on sapphire substrate by the CVD process.

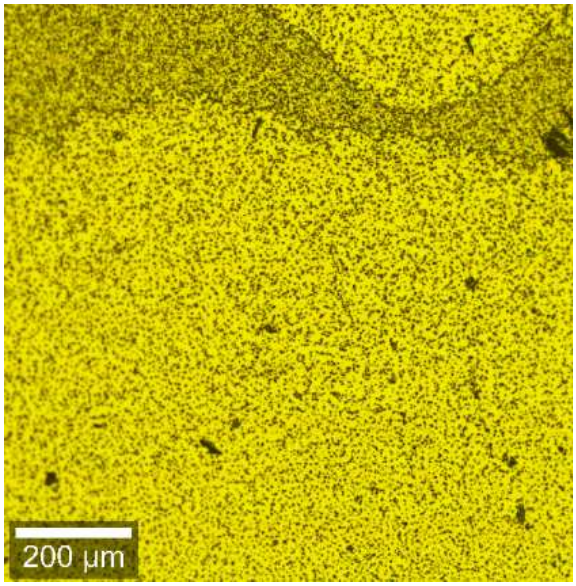

Figure 4.12: Stitching images of region of FeS_2 material synthesized at the annealing temperature of 800 °C.

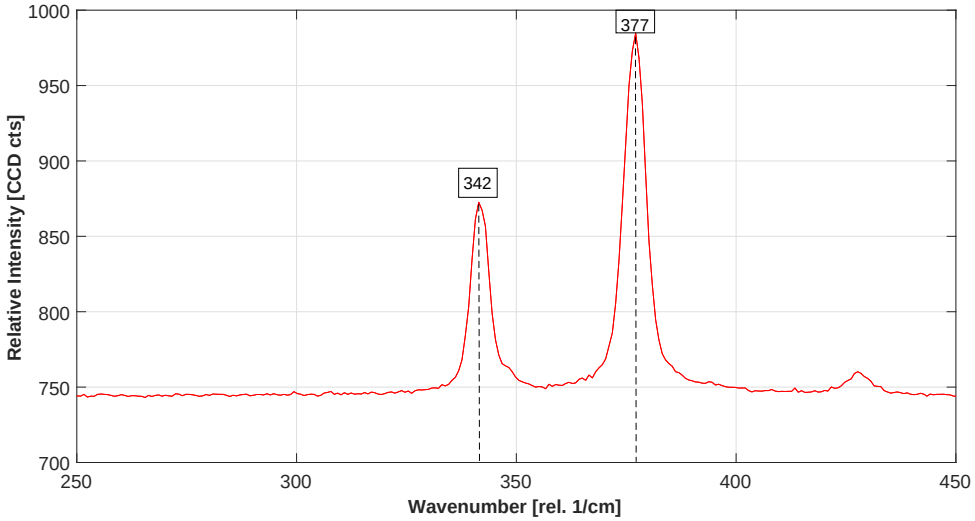

Figure 4.13: Raman spectrum of FeS_2 material synthesized at the annealing temperature of 800 °C.

The SEM image of FeS_2 is represented in Figure 4.14. According to the research published earlier, properly synthesized FeS_2 is expected to produce hexagonal flakes [11]. In our SEM characterization results, shown in Figure 4.14, we observed some hexagonal-shaped flakes which confirm the growth of FeS_2 on the sapphire substrate.

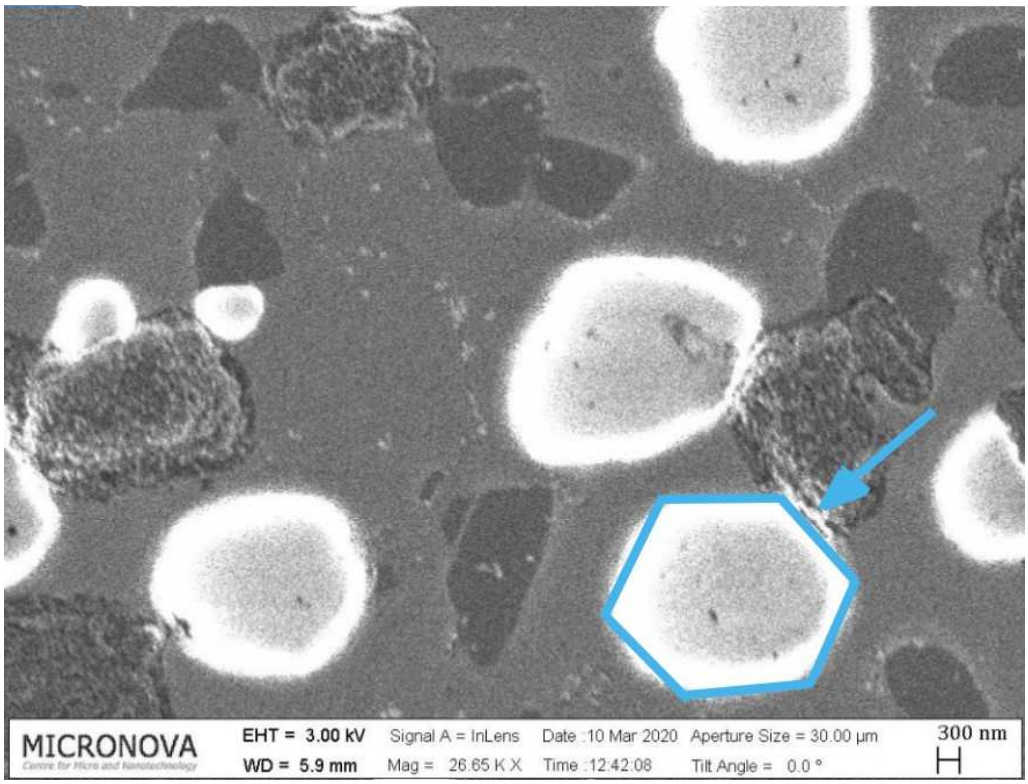

Figure 4.14: SEM image of FeS_2 material synthesized at the annealing temperature of 800 °C.

4.1.4 Other samples

Some of the other samples such as TiS_2 and HfS_2 are also briefly discussed in this thesis. Although these materials have shown some promise in their synthesis, still some more research and varied growth parameters are required to be tested to optimize their synthesis for the FET applications.

TiS_2 thin film material synthesized at the annealing temperature of 800 °C
The thin-film sample of TiS_2 was synthesized at the annealing temperature of 800 °C with an argon gas flow rate of 20 sccm during the CVD process. Figure 4.15 represents the stitching images of synthesized TiS_2 material captured by the Raman tool. As observed by the different color shades in the two figures, the pictures represent growth of TiS_2 on different thickness of gold on the sapphire substrate. Although previous literature report has suggested that the Raman peaks of the few-layered flakes are observed at 230 rel. cm^{-1} and 329 rel. cm^{-1}, in our experiments we obtained some response at 240 rel. cm^{-1} but not at around 329 rel. cm^{-1} as shown in Figure 4.16 [33]. Thus, in our experimental synthesis and characterization, it is suggested that we have some traces of TiS_2 growth on the sapphire substrate, but it still requires further experiments to polish the results and synthesis.

HfS_2 thin film material synthesized at the annealing temperature of 800 °C
HfS_2 was synthesized at the annealing temperature of 800 °C and 50 sccm of argon gas flow rate during the CVD process. SEM images of thin film of HfS_2 are represented in Figure 4.17. The previous literature paper has suggested that as-synthesized HfS_2 are hexagonal-like flakes [34, 35]. In our experimental characterization, it has been revealed that HfS_2 material has some hexagonal-like flakes as shown in Figure 4.17. Since some of the flakes are also observed to be circular-like shaped as well, we can conclude that further improvement in the synthesis technique is required for better growth of HfS_2 by the CVD process.

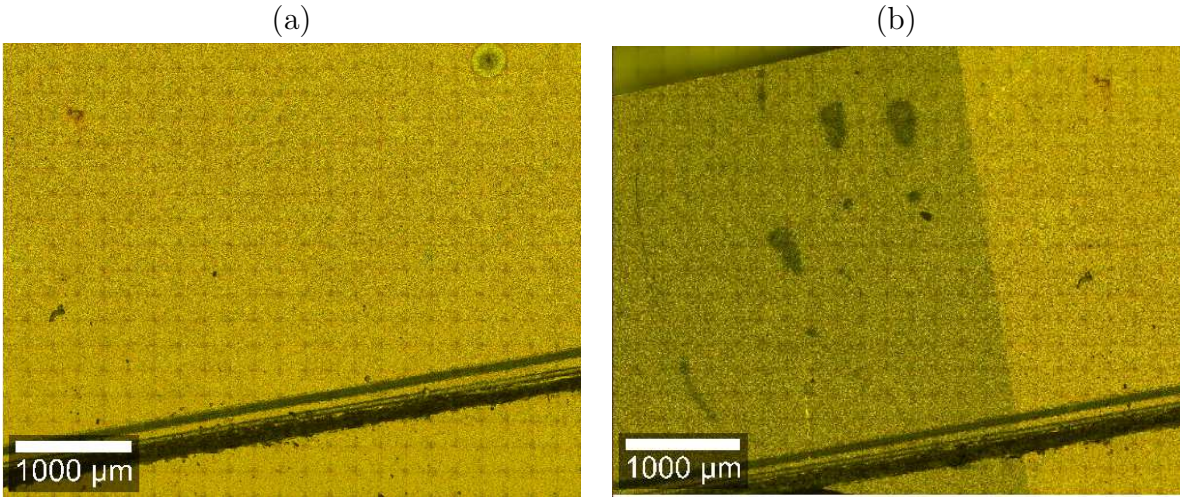

Figure 4.15: Stitching image of a region of TiS_2 material synthesized at the annealing temperature of 800 °C with (a) low thickness of gold on sapphire substrate, (b) high thickness of gold on sapphire substrate.

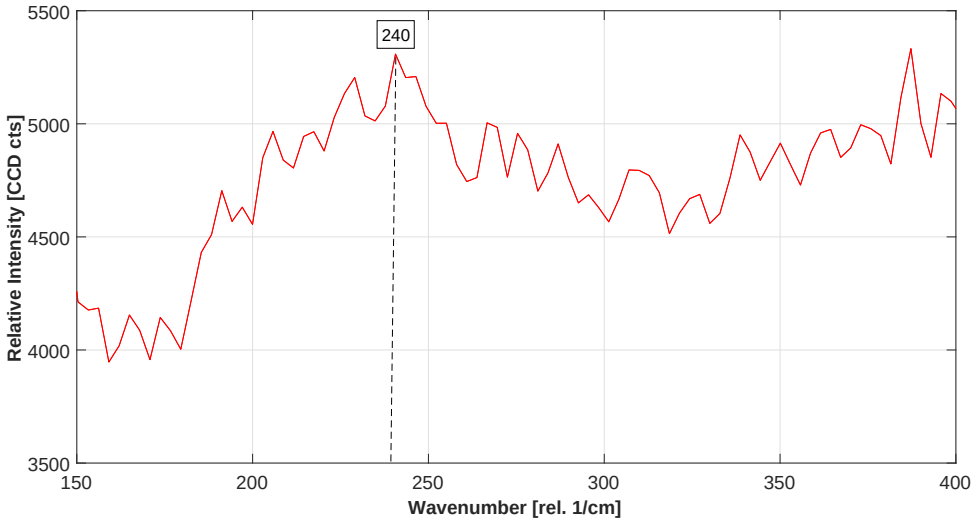

Figure 4.16: Raman spectrum of FeS_2 material synthesized at the annealing temperature of 800 °C.

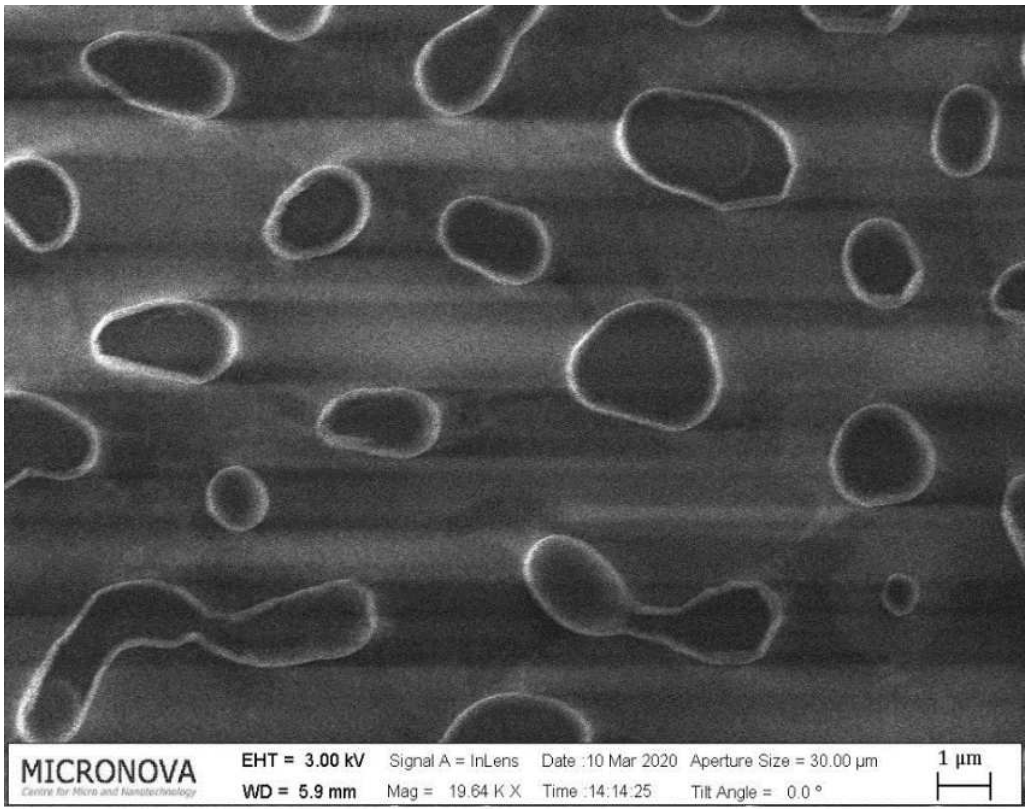

Figure 4.17: SEM image of HfS_2 material synthesized at the annealing temperature of 800 °C.

4.2 Optical characterization

It is significant to understand and enhance the photoluminescence (PL) behavior in 2D TMDs such as in MoS_2 for pursuing optoelectronic applications. To obtain the best optical responses in our experimental work, high-quality thin layered MoS_2 materials were synthesized, and their intrinsic PL performances were also explored. As discussed in the previous sections, we synthesized and characterized MoS_2 samples at the annealing temperatures of 900 °C, 800 °C, and 750 °C. This section focuses on their PL response at room temperature and the effect of temperatures (from +23 °C to -196 °C) on the shift of their peak wavelengths.

4.2.1 Photoluminescence measurements of 2D materials

Figure 4.18a, 4.18b, and 4.18c represents the PL spectrums of MoS_2 materials synthesized at the annealing temperatures of 900 °C, 800 °C, and 750 °C, respectively. According to the earlier literature reviews, it has been observed that the thin film of MoS_2 shows a PL peak at a wavelength of around 673 nm (1.84 eV) [31,36]. This 1.84 eV energy primarily explains the energy difference between the levels of two electron states involved in the transition as electron moves from lower energy level to the higher energy level due to the excitation by the incoming laser light. In our experimental setup, we have used a laser light of 532 nm with 1.5 mW power for the excitation of electrons, and the material's responses are captured and measured by the Raman tool.

Experimental results for MoS_2 synthesized at the annealing temperature of 900 °C show the PL spectrum with the main peak at the wavelength of around 666 nm as shown in Figure 4.18a, while the main peaks for the MoS_2 samples synthesized at the annealing temperature of 800 °C and 750 °C are observed at the wavelengths of around 680 nm and 631 nm, respectively, as represented in Figures 4.18b and 4.18c. Thus, this result of the PL response that we have observed through our experimental setup is also in accordance with the expected results published earlier.

(a)

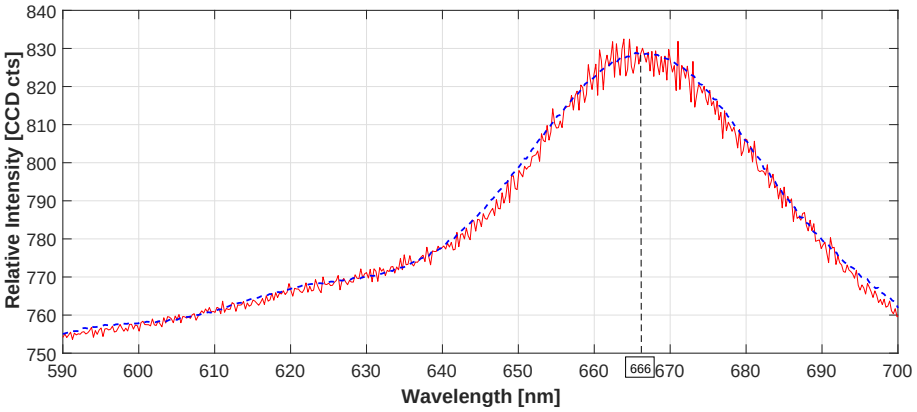

(b)

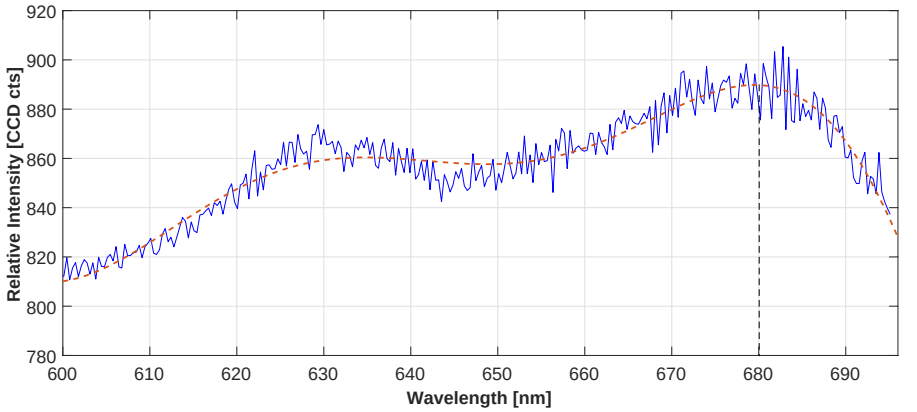

(c)

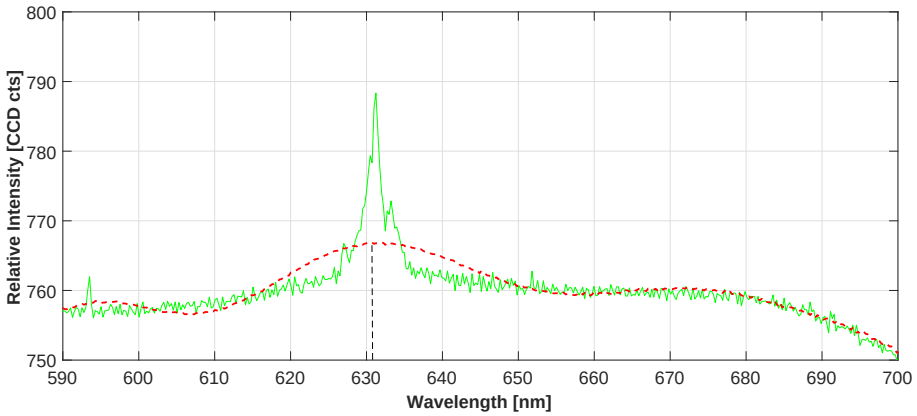

Figure 4.18: PL response of MoS_2 sample synthesized at (a) 900 °C, (b) 800 °C, and (c) 750 °C.

4.2.2 Variation of temperature in PL measurements

In the previous section, we discussed the PL response of MoS_2 samples by the Raman spectrometry at room temperature. Although for the most practical applications of FETs, devices are typically required to operate under room temperature and pressure, PL responses and material's properties with the change of their operating temperatures can give valuable information about the material's quality and characteristics. According to the literature review paper published earlier, it was observed that with rising temperature, the peak broadens and shifts to lower energy (longer wavelengths) [37].

In our experiments, we used the Linkam measurement setup, discussed in Chapter 2, to adjust and control the temperatures of our samples down to liquid nitrogen temperatures. The changes in their properties and peak wavelengths of PL responses are measured using the Raman tool. Although the PL measurements were performed with other TMDs samples as well, we discuss and summarize only the results of the MoS_2 sample that was synthesized at 900 °C with 50 sccm of gas flow rate. The effect of temperature change on the PL response is represented in 4.19, where the PL response has been measured and plotted for +23 °C, -100 °C, and -196 °C. We can observe from the graphs that the spectrum broadens and peak wavelength shifts to longer wavelengths (lower energy) as the temperature is increased from -196 °C to +23 °C. The wavelength of the main peak can be observed at around 650 nm at -196 °C; it shifts to 660 nm at -100 °C, and 666 nm at +23 °C. Thus, this result also confirms the discussion mentioned in Ref. [37].

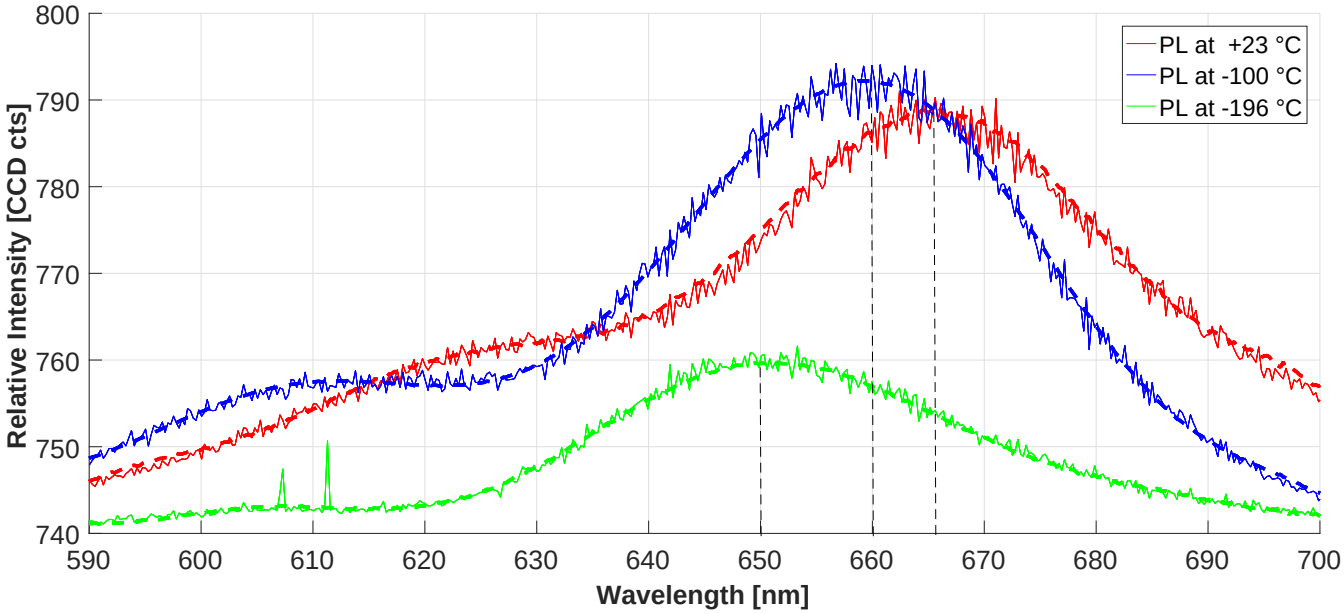

Figure 4.19: PL variation with variation in temperature (from +23 °C to -196 °C) for MoS_2 sample.

Chapter V
Conclusions

It is important to optimize the quality of 2D materials used in the fabrication of FETs. This thesis has focused on the synthesis and characterization of various 2D materials (TMDs) such as MoS_2, CrS_2, FeS_2, TiS_2, and HfS_2. Different parameters were tested in the CVD process to produce high-quality growth of 2D materials. Using SEM and Raman analysis, it is determined that a thin layer of MoS_2 can be synthesized at the annealing temperature of 750 °C using the CVD process. However, other experimented MoS_2 samples synthesized at other annealing temperatures also showed some prominence in their material growths.

Other 2D materials such as CrS_2 and FeS_2 also provided reasonable results in synthesis. Materials such as TiS_2 and HfS_2 showed some promise in the synthesis, but they would still require some research for enhancing their quality. The experimental characterization results of these materials have also been discussed and compared with the results of earlier published papers to determine and confirm the proper synthesis of our materials.

In addition to the SEM and Raman analyses, optical characterizations have also been explored. PL measurements were performed and discussed for three MoS_2 samples synthesized at different annealing temperatures. Moreover, PL behavior of MoS_2 sample was observed by decreasing the operating temperature down to liquid nitrogen temperature. It was also observed that the spectrum broadens and peak wavelength shifts to longer wavelengths as the temperature is increased from -196 °C to +23 °C. Hence, due to their remarkable properties of high electron mobility, high switching ratio, combined with the typically direct band-gap, TMDs are suitable for various applications in optoelectronics.

References

[1] K. S. Novoselov, A. K. Geim, S. V. Morozov, D. Jiang, Y. Zhang, S. V. Dubonos, I. V. Grigorieva, and A. A. Firsov, "Electric field effect in atomically thin carbon films," *Science* **306**, 666–669 (2004).

[2] C. Berger, Z. Song, T. Li, X. Li, A. Y. Ogbazghi, R. Feng, Z. Dai, A. N. Marchenkov, E. H. Conrad, P. N. First, et al., "Ultrathin epitaxial graphite: 2D electron gas properties and a route toward graphene-based nanoelectronics," *The Journal of Physical Chemistry B* **108**, 19912–19916 (2004).

[3] F. Schwierz, "Graphene transistors: status, prospects, and problems," *Proceedings of the IEEE* **101**, 1567–1584 (2013).

[4] L. Li, Y. Yu, G. J. Ye, Q. Ge, X. Ou, H. Wu, D. Feng, X. H. Chen, and Y. Zhang, "Black phosphorus field-effect transistors," *Nature Nanotechnology* **9**, 372 (2014).

[5] M. Chhowalla, H. S. Shin, G. Eda, L.-J. Li, K. P. Loh, and H. Zhang, "The chemistry of two-dimensional layered transition metal dichalcogenide nanosheets," *Nature Chemistry* **5**, 263 (2013).

[6] Z. Y. Al Balushi, K. Wang, R. K. Ghosh, R. A. Vilá, S. M. Eichfeld, J. D. Caldwell, X. Qin, Y.-C. Lin, P. A. DeSario, G. Stone, et al., "Two-dimensional gallium nitride realized via graphene encapsulation," *Nature Materials* **15**, 1166–1171 (2016).

[7] B. Radisavljevic, A. Radenovic, J. Brivio, V. Giacometti, and A. Kis, "Single-layer MoS 2 transistors," *Nature Nanotechnology* **6**, 147 (2011).

[8] J. Xiao, M. Long, X. Li, H. Xu, H. Huang, and Y. Gao, "Theoretical prediction of electronic structure and carrier mobility in single-walled MoS 2 nanotubes," *Scientific Reports* **4**, 1–7 (2014).

[9] S. H. Gu, V. Nicolas, A. Lalis, N. Sathirapongsasuti, and R. Yanagihara, "Complete genome sequence and molecular phylogeny of a newfound hantavirus harbored by the Doucet's musk shrew (Crocidura douceti) in Guinea," *Infection, Genetics and Evolution* **20**, 118–123 (2013).

[10] T. Sakamoto, H. Sunamura, H. Kawaura, T. Hasegawa, T. Nakayama, and M. Aono, "Nanometer-scale switches using copper sulfide," *Applied Physics Letters* **82**, 3032–3034 (2003).

[11] A. Shivayogimath, J. D. Thomsen, D. M. Mackenzie, M. Geisler, R.-M. Stan, A. J. Holt, M. Bianchi, A. Crovetto, P. R. Whelan, A. Carvalho, et al., "A universal approach for the synthesis of two-dimensional binary compounds," *Nature Communications* **10**, 1–7 (2019).

[12] J. Garcia and D. De Lima, "Assali, LVC; Justo. JF," *Group N Graphene-and Graphane-Like Nanosheets. J. Chem. Phys. C* **115**, 13242–13246 (2011).

[13] M. Ashton, J. Paul, S. B. Sinnott, and R. G. Hennig, "Topology-scaling identification of layered solids and stable exfoliated 2D materials," *Physical Review Letters* **118**, 106101 (2017).

[14] J. J.-S. Huang, Y.-H. Jan, H. Chang, C.-J. Ni, E. Chou, S.-K. Lee, H.-S. Chen, and J.-W. Shi, "Nanoscale III-V Semiconductor Photodetectors for High-Speed Optical Communications," in *Two-dimensional Materials for Photodetector* (IntechOpen, 2017).

[15] R. Clark, "Real World Graphene: Industrial Applications for the 21st Century," (2017).

[16] W. Ren and H.-M. Cheng, "The global growth of graphene," *Nature Nanotechnology* **9**, 726–730 (2014).

[17] X. Liu, J. Hu, C. Yue, N. Della Fera, Y. Ling, Z. Mao, and J. Wei, "High performance field-effect transistor based on multilayer tungsten disulfide," *ACS Nano* **8**, 10396–10402 (2014).

[18] 2D Materials: An Introduction to Two-Dimensional Materials, https://www.ossila.com/pages/introduction-2d-materials (visited on 2020-03-24).

[19] W. Tang, S. Rassay, and N. Ravindra, "Electronic & Optical properties of transition-metal dichalcogenides," *Madridge Journal of Nanotechnology and Nanoscience* **2**, 59–65 (2017).

[20] J. Yu, J. Li, W. Zhang, and H. Chang, "Synthesis of high quality two-dimensional materials via chemical vapor deposition," *Chemical science* **6**, 6705–6716 (2015).

[21] EDX analysis in SEM: the principle explained, https://blog.phenom-world.com/edx-analysis-sem (visited on 2020-04-02).

[22] M. Xia, "A review on applications of two-dimensional materials in surface-enhanced Raman spectroscopy," *International Journal of Spectroscopy* **2018** (2018).

[23] M. A. McCord and M. J. Rooks, "SPIE handbook of microlithography, micromachining and microfabrication," in *SPIE, Bellingham* (2000).

[24] J. G. R. Sereni, "Reference module in materials science and materials engineering," (2016).

[25] G. Rius Suñé, *Electron beam lithography for nanofabrication* (Universitat Autònoma de Barcelona,, 2008).

[26] Y. Gao, Z. Liu, D.-M. Sun, L. Huang, L.-P. Ma, L.-C. Yin, T. Ma, Z. Zhang, X.-L. Ma, L.-M. Peng, et al., "Large-area synthesis of high-quality and uniform monolayer WS 2 on reusable Au foils," *Nature Communications* **6**, 8569 (2015).

[27] I. Song, C. Park, M. Hong, J. Baik, H.-J. Shin, and H. C. Choi, "Patternable large-scale molybdenium disulfide atomic layers grown by gold-assisted chemical vapor deposition," *Angewandte Chemie International Edition* **53**, 1266–1269 (2014).

[28] J. S. Lee, S. H. Choi, S. J. Yun, Y. I. Kim, S. Boandoh, J.-H. Park, B. G. Shin, H. Ko, S. H. Lee, Y.-M. Kim, et al., "Wafer-scale single-crystal hexagonal boron nitride film via self-collimated grain formation," *Science* **362**, 817–821 (2018).

[29] Y. Shi, H. Li, and L.-J. Li, "Recent advances in controlled synthesis of two-dimensional transition metal dichalcogenides via vapour deposition techniques," *Chemical Society Reviews* **44**, 2744–2756 (2015).

[30] F. Ghasemi, R. Frisenda, D. Dumcenco, A. Kis, D. Perez de Lara, and A. Castellanos-Gomez, "High throughput characterization of epitaxially grown single-layer MoS2," *Electronics* **6**, 28 (2017).

[31] K. Gołasa, M. Grzeszczyk, K. Korona, R. Bożek, J. Binder, J. Szczytko, A. Wysmołek, and A. Babiński, "Optical Properties of Molybdenum Disulfide (MoS 2).," *Acta Physica Polonica, A.* **124** (2013).

[32] B. Yuan, W. Luan, and S.-t. Tu, "One-step synthesis of cubic FeS 2 and flower-like FeSe 2 particles by a solvothermal reduction process," *Dalton transactions* **41**, 772–776 (2012).

[33] M. A. Bissett, S. D. Worrall, I. A. Kinloch, and R. A. Dryfe, "Comparison of two-dimensional transition metal dichalcogenides for electrochemical supercapacitors," *Electrochimica Acta* **201**, 30–37 (2016).

[34] C. Yan, L. Gan, X. Zhou, J. Guo, W. Huang, J. Huang, B. Jin, J. Xiong, T. Zhai, and Y. Li, "Space-confined chemical vapor deposition synthesis of ultrathin HfS2 flakes for optoelectronic application," *Advanced Functional Materials* **27**, 1702918 (2017).

[35] S. Zhou, L. Gan, D. Wang, H. Li, and T. Zhai, "Space-confined vapor deposition synthesis of two dimensional materials," *Nano Research* **11**, 2909–2931 (2018).

[36] S. Catalán-Gómez, S. Garg, A. Redondo-Cubero, N. Gordillo, A. de Andrés, F. Nucciarelli, S. Kim, P. Kung, and J. L. Pau, "Photoluminescence enhancement of monolayer MoS 2 using plasmonic gallium nanoparticles," *Nanoscale Advances* **1**, 884–893 (2019).

[37] T. Korn, S. Heydrich, M. Hirmer, J. Schmutzler, and C. Schüller, "Low-temperature photocarrier dynamics in monolayer MoS2," *Applied Physics Letters* **99**, 102109 (2011).